Supplementary Material

1 Appendix 1: Detail of the Critical Pseudo-Multi Impulse Analysis

In this appendix, the details of the critical pseudo-multi impulse analysis (section 2.1) is described as follows.

1.1 First pseudo impulsive lateral force

At time $t = {}_1t_p \left({}_1t_p > 0 \right)$, the first pseudo impulsive lateral force acts on the building model as shown in Figure 1. Note that, before the action of the first pseudo impulsive force on the building model ($t < {}_1t_p$), the building model is in a stationary state ($\mathbf{d}(t) = \mathbf{0}$, $\mathbf{v}(t) = \mathbf{0}$, $\mathbf{a}(t) = \mathbf{0}$). The equivalent velocity of the first modal response just after the action of the first pseudo impulsive lateral force ($\tilde{V}_1^*\left({}_1t_p\right)$) is calculated using Eq. (A1):

$$\tilde{V}_1^*\left({}_1t_p\right) = -{}_1\Delta V_g\,, \tag{A1}$$

and the corresponding velocity vector ($\tilde{\mathbf{v}}\left({}_1t_p\right)$) is calculated using Eq. (A2):

$$\tilde{\mathbf{v}}\left({}_1t_p\right) = {}_1\Gamma_1\,{}_1\boldsymbol{\varphi}_1 \tilde{V}_1^*\left({}_1t_p\right) = -{}_1\Gamma_1\,{}_1\boldsymbol{\varphi}_1\,{}_1\Delta V_g\,, \tag{A2}$$

where ${}_1\Gamma_1\,{}_1\boldsymbol{\varphi}_1$ is the first mode vector at the initial stage. The increment of input energy of the first modal response (${}_1\Delta E_1^*$) is calculated via Eq. (A3):

$${}_1\Delta E_1^* = \frac{1}{2}\,{}_1M_1^*\left\{\tilde{V}_1^*\left({}_1t_p\right)\right\}^2 = \frac{1}{2}\,{}_1M_1^*\,{}_1\Delta V_g^{\,2}\,, \tag{A3}$$

where ${}_1M_1^*$ is the first modal mass at the initial stage. The cumulative input energy of the first modal response (${}_1E_1^*$) is calculated via Eq. (A4):

$${}_1E_{I1}^* = {}_1\Delta E_1^*\,. \tag{A4}$$

To calculate the response after the action of the first pseudo impulsive lateral force, the equivalent velocity ($V_1^*(t)$) and velocity vector ($\mathbf{v}(t)$) are updated via Eq. (A5):

$$V_1^*\left({}_1t_p + 0\right) \leftarrow \tilde{V}_1^*\left({}_1t_p\right), \mathbf{v}\left({}_1t_p + 0\right) \leftarrow \tilde{\mathbf{v}}\left({}_1t_p\right). \tag{A5}$$

In addition, the counting number of pulsive inputs (k) is set to $k = 1$.

1.2 Free vibration after the first pseudo impulsive lateral force

After the action of the first pseudo impulsive lateral force, the building model oscillates without external forces (free vibration) until the arrival of the second pseudo impulsive lateral force. The kinetic energy, the damping dissipated energy, the cumulative strain energy, and the cumulative input energy of the first modal response (E_{K1}^*, E_{D1}^*, E_{S1}^*, and E_{I1}^*, respectively) are expressed as shown in Eqs. (A6)–(A9):

$$E_{K1}^*(t) = \frac{1}{2} M_1^* \left\{ V_1^*(t) \right\}^2 , \tag{A6}$$

$$E_{D1}^*(t) = \int_0^t \Gamma_1 \boldsymbol{\varphi}_1{}^{\mathbf{T}} \mathbf{f}_{\mathbf{D}}(t) V_1^*(t)\, dt , \tag{A7}$$

$$E_{S1}^*(t) = \int_0^t \Gamma_1 \boldsymbol{\varphi}_1{}^{\mathbf{T}} \mathbf{f}_{\mathbf{R}}(t) V_1^*(t)\, dt , \tag{A8}$$

$$E_{I1}^*(t) = \frac{1}{2} {}_1M_1^* {}_1\Delta V_g^2 = {}_1E_{I1}^* . \tag{A9}$$

The first pseudo impulsive lateral force is proportional to the first mode vector, and thus the building model oscillates predominantly in the first mode. Therefore, the kinetic energy, the damping dissipated energy, the cumulative strain energy, and the cumulative input energy (E_K, E_D, E_S, and E_I, respectively) are approximated as shown in Eq. (A10):

$$\begin{cases} E_K(t) \approx E_{K1}^*(t) \\ E_D(t) \approx E_{D1}^*(t) \\ E_S(t) \approx E_{S1}^*(t) \\ E_I(t) \approx E_{I1}^*(t) \end{cases} . \tag{A10}$$

Note that the first mode vector ($\Gamma_1 \boldsymbol{\varphi}_1$) updates any step according to Eq. (A11) until $D_1^*(t)$ reaches its local peak (${}_1D_{1\,peak}^*\,(<0)$).

$$\Gamma_1 \boldsymbol{\varphi}_1 \leftarrow \frac{1}{D_1^*(t_{\max})} \mathbf{d}(t_{\max}) . \tag{A11}$$

The effective first modal mass (M_1^*) is then re-calculated according to Eq. (A12). The time ${}_1t_{peak}$ is defined as the time when $D_1^*(t)$ reaches ${}_1D_{1\,peak}^*$.

$$M_1^* = \Gamma_1^2 \boldsymbol{\varphi}_1{}^{\mathbf{T}} \mathbf{M} \boldsymbol{\varphi}_1 , \tag{A12}$$

The timing of the action of the second pseudo impulsive lateral force (${}_2t_p > {}_1t_p$) is determined from the following conditions:

$$A_{r1}^{*}\left({}_2t_p\right) = 0 . \tag{A13}$$

Equation (A13) is equivalent to the condition of critical timing given by Akehashi and Takewaki (2021, 2022). In Akehashi and Takewaki (2021), the critical timing of the second pseudo impulsive lateral force is determined as the timing which maximize the energy input by the second input. Following the Akehashi and Takewaki (2021), consider the case when the pseudo impulsive lateral force is proportional to the influence vector ($\boldsymbol{\iota}$) defined as Eq. (A15):

$$\boldsymbol{\iota} = \sum_{j=1}^{N} q_j \Gamma_j \boldsymbol{\varphi}_{\mathbf{j}} . \tag{A14}$$

The condition of the critical timing of the second pseudo impulsive lateral force is expressed as

$$\sum_{j=1}^{N} q_j M_j^{*} A_{rj}^{*}\left({}_2t_p\right) = 0 . \tag{A15}$$

In Eq. (A15), $A_{rj}^{*}(t)$ is the equivalent relative acceleration of the j-th modal response. For the case of this study, when the influence vector ($\boldsymbol{\iota}$) equals to the first mode vector ($\Gamma_j \boldsymbol{\varphi}_{\mathbf{j}}$), the coefficient q_j is zero for $2 \le j \le N$ and q_1 equals 1. Therefore, Eq. (A16) can be rewritten as Eq. (A16).

$$M_1^{*} A_{r1}^{*}\left({}_2t_p\right) = 0 . \tag{A16}$$

The condition expressed as Eq. (A16) is equivalent to Eq. (A13), because the effective first modal mass (M_1^{*}) is nonzero value.

1.3 Pseudo impulsive lateral force

At time $t = {}_{k+1}t_p$ ($1 \le k \le N_p - 1$), the next pseudo impulsive lateral force acts on the building model, as shown in Figure 1. The equivalent velocity of the first modal response just after the action of the next pseudo impulsive lateral force ($\tilde{V}_1^{*}\left({}_{k+1}t_p\right)$) is calculated via Eq. (A17):

$$\tilde{V}_1^{*}\left({}_{k+1}t_p\right) = V_1^{*}\left({}_{k+1}t_p - 0\right) - {}_{k+1}\Delta V_g . \tag{A17}$$

Here, $V_1^{*}\left({}_{k+1}t_p - 0\right)$ is the equivalent velocity of the first modal response just before the action of the next pseudo impulsive lateral force. Assuming that the velocity vector just before the action of the next pseudo impulsive lateral force ($\mathbf{v}\left({}_{k+1}t_p - 0\right)$) can be approximated by the first modal response, the corresponding velocity vector ($\tilde{\mathbf{v}}\left({}_{k+1}t_p\right)$) can be expressed as Eq. (A18):

$$\tilde{\mathbf{v}}\left({}_{k+1}t_p\right) = \mathbf{v}\left({}_{k+1}t_p - 0\right) - \Gamma_1 \boldsymbol{\varphi}_{\mathbf{1}}\, {}_{k+1}\Delta V_g \approx \Gamma_1 \boldsymbol{\varphi}_{\mathbf{1}} \tilde{V}_1^{*}\left({}_{k+1}t_p\right) . \tag{A18}$$

The increment of the input energy of the first modal response (${}_{2}\Delta E_1^*$) is calculated via Eq. (A19):

$$ {}_{k+1}\Delta E_1^* = \frac{1}{2} M_1^* \left[\left\{ \tilde{V}_1^* \left({}_{k+1}t_p \right) \right\}^2 - \left\{ V_1^* \left({}_{k+1}t_p - 0 \right) \right\}^2 \right] = \frac{1}{2} M_1^* \, {}_{k+1}\Delta V_g^{\,2} \left\{ 1 + \frac{2V_1^* \left({}_{k+1}t_p - 0 \right)}{{}_{k+1}\Delta V_g} \right\}. \quad \text{(A19)} $$

The cumulative input energy of the first modal response just after the action of the next pseudo impulsive lateral force (${}_{k+1}E_{I1}^*$) is calculated via Eq. (A20):

$$ {}_{k+1}E_{I1}^* = {}_{k}E_{I1}^* + {}_{k+1}\Delta E_1^*. \quad \text{(A20)} $$

To calculate the response after the action of the second pseudo impulsive lateral force, the equivalent velocity ($V_1^*(t)$) and the velocity vector ($\mathbf{v}(t)$) are updated via Eq. (A21):

$$ V_1^* \left({}_{k+1}t_p + 0 \right) \leftarrow \tilde{V}_1^* \left({}_{k+1}t_p \right), \mathbf{v} \left({}_{k+1}t_p + 0 \right) \leftarrow \tilde{\mathbf{v}} \left({}_{k+1}t_p \right). \quad \text{(A21)} $$

In addition, the counting number of the pulsive inputs (k) is updated such that $k \leftarrow k+1$.

1.4 Free vibration

After the action of the k-th pseudo impulsive lateral force, the building model oscillates without external forces (free vibration). The following response depends on k and N_p.

In the case in which k is smaller than N_p, the free vibration of the building model continues until the action of the next pseudo impulsive lateral force. During the free vibration, the first mode vector ($\Gamma_1\boldsymbol{\varphi}_1$) updates any step according to Eq. (A12) until $D_1^*(t)$ reaches its local peak (${}_{k}D_{1\,peak}^*$ shown in Figure 1). The effective first modal mass (M_1^*) is then re-calculated according to Eq. (A13). The time ${}_{k}t_{peak}$ is defined as the time when $D_1^*(t)$ reaches ${}_{k}D_{1\,peak}^*$. The timing of the action of the next pseudo impulsive lateral force (${}_{k+1}t_p > {}_{k}t_p$) is determined from the following conditions (Eq. (A22)):

$$ A_{r1}^* \left({}_{k+1}t_p \right) = 0. \quad \text{(A22)} $$

At time $t = {}_{k+1}t_p$, the next pseudo impulsive lateral force acts as prescribed in Section 1.3 of this supplementary material.

When k equals N_p, the free vibration of the building model continues until $t = t_{end}$. The time ${}_{N_p}t_{peak}$ is defined as the time when $D_1^*(t)$ reaches ${}_{N_p}D_{1\,peak}^*$.

Supplementary Figure 1 shows the flow of the critical PMI analysis. This flow is based on the flow of the critical PDI analysis presented in Fujii (2024).

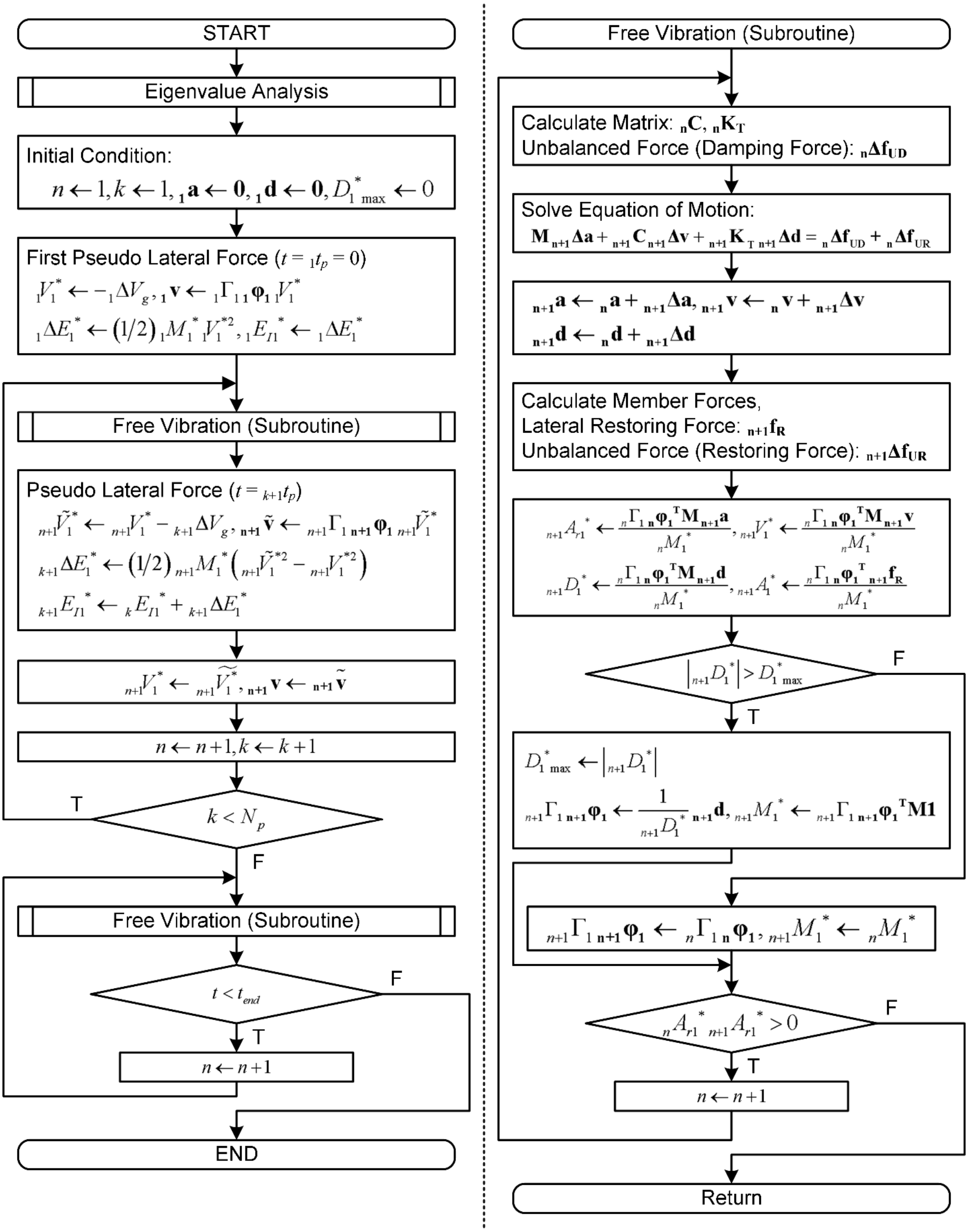

Supplementary Figure 1. Flow of the critical PMI analysis.

2 Appendix 2: Simplified Equations for Calculating the Energy Dissipation Capacity During a Half Cycle of the Structural Response

It is assumed that the peak equivalent displacement of the first modal response ($D_{1\ \max}^{*}$) occurs when the maximum momentary energy input ($\Delta E_{1\ \max}^{*} / M_1^{*}$) occurs. Following Fujii and Shioda (2023), the energy dissipation capacity during a half cycle of the structural response is expressed as

$$\frac{\Delta E_{1\ \max}^{*}}{M_1^{*}} = \frac{\Delta E_{\mu 1 f}^{\ *}}{M_1^{*}} + \frac{\Delta E_{\mu 1 d}^{\ *}}{M_1^{*}} + \frac{\Delta E_{D1}^{\ *}}{M_1^{*}}. \tag{A23}$$

In Eq. (A23), $\Delta E_{\mu 1 f}^{\ *} / M_1^{*}$ and $\Delta E_{\mu 1 d}^{\ *} / M_1^{*}$ are the contributions from the hysteretic dissipated energies of the RC MRFs and SDCs, respectively, while $\Delta E_{D1}^{\ *} / M_1^{*}$ is the contribution from viscous damping.

Supplemental Figure 2 shows the simplified model for calculating $\Delta E_{\mu 1 f}^{\ *} / M_1^{*}$ and $\Delta E_{\mu 1 d}^{\ *} / M_1^{*}$. In the figure, $A_{1f}^{\ *}$ and $A_{1d}^{\ *}$ are the contributions of the RC MRFs and SDCs, respectively, to the equivalent acceleration of the first modal response (A_1^{*}). Here, the $A_{1f}^{\ *} - D_1^{*}$ and $A_{1d}^{\ *} - D_1^{*}$ relationships are idealized by bilinear curves, where the "yield" point of the idealized $A_{1f}^{\ *} - D_1^{*}$ relationship is YF($D_{1yf}^{\ *}$, $A_{1yf}^{\ *}$) and that of the idealized $A_{1d}^{\ *} - D_1^{*}$ relationship is YD($D_{1yd}^{\ *}$, $A_{1yd}^{\ *}$). In addition, μ_f and μ_d denote the global ductility of the RC MRFs and SDCs, respectively, which are defined in Eq. (A24):

$$\mu_f = D_{1\ \max}^{*} / D_{1yf}^{\ *}, \mu_d = D_{1\ \max}^{*} / D_{1yd}^{\ *}. \tag{A24}$$

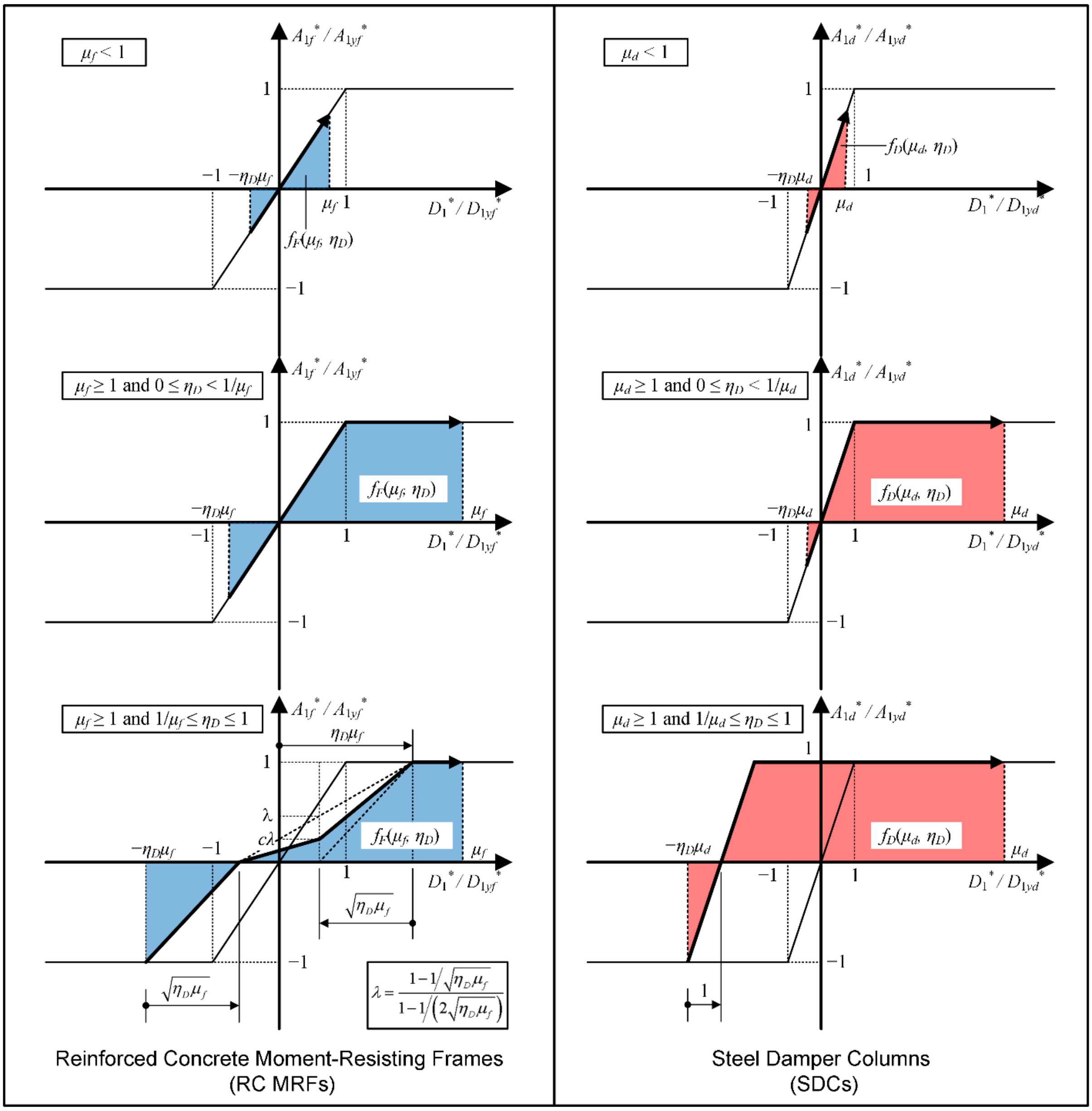

Supplementary Figure 2. Simplified model for calculating the hysteretic dissipated energy during a half cycle of structural response.

The contribution of the hysteretic dissipated energy of the RC MRFs is calculated using Eq (A25):

$$\frac{\Delta E_{\mu 1f}^{\ *}}{M_1^{\ *}} = A_{1yf}^{\ *} D_{1yf}^{\ *} \widetilde{f_F}\left(\mu_f\right). \tag{A25}$$

The function $\widetilde{f_F}\left(\mu_f\right)$ is defined by Eq. (A26):

$$\widetilde{f_F}\left(\mu_f\right) = \int_0^1 f_F\left(\mu_f, \eta_D\right) d\eta_D\,, \tag{A26}$$

where η_D is the ratio of the displacements in the positive and negative directions. Given the left panel of Supplemental Figure 2, $f_F\left(\mu_f,\eta_D\right)$ is calculated as

$$f_F\left(\mu_f,\eta\right)=\begin{cases}\dfrac{1}{2}{\mu_f}^2\left(1-{\eta_D}^2\right) & 0\le\mu_f\le 1\\ \mu_f-\dfrac{1}{2}\left\{1+\left(\eta_D\mu_f\right)^2\right\} & \mu_f\ge 1 \text{ and } 0\le\eta_D\le\dfrac{1}{\mu_f}\\ \mu_f\left(1-\eta_D\right)+c\left(\eta_D\mu_f-\sqrt{\eta_D\mu_f}\right) & \mu_f\ge 1 \text{ and } \dfrac{1}{\mu_f}\le\eta_D\le 1\end{cases}. \tag{A27}$$

Note that, in Eq. (A27), the influence of the pinching behavior of the RC members on the hysteretic energy dissipation in a half cycle of the structural response is considered by the parameter c. This is an updated version of this equation, as compared with previous studies (Fujii, 2022; Fujii and Shioda, 2023). By substituting Eq. (A27) into Eq. (A26), the function $\widetilde{f_F}\left(\mu_f\right)$ is calculated as

$$\widetilde{f_F}\left(\mu_f\right)=\begin{cases}\dfrac{1}{3}{\mu_f}^2 & 0\le\mu_f\le 1\\ \dfrac{1}{2}\left(1+c\right)\mu_f-\dfrac{2}{3}c\sqrt{\mu_f}-\dfrac{1}{6\mu_f}\left(1-c\right) & \mu_f\ge 1\end{cases}. \tag{A28}$$

Note that Eq. (A28) is consistent with the equation in Fujii and Shioda (2023): by substituting c = 1 into Eq. (A28), the same equation for the perfectly non-pinching RC MRFs (Fujii and Shioda, 2023) is obtained. Similarly, the contribution of the hysteretic dissipated energy of the SDCs is calculated using Eq (A29):

$$\frac{\Delta {E_{\mu 1d}}^*}{{M_1}^*}={A_{1yd}}^*{D_{1yd}}^*\widetilde{f_D}\left(\mu_d\right). \tag{A29}$$

The function $\widetilde{f_D}\left(\mu_d\right)$ is defined as in Eq. (A30):

$$\widetilde{f_D}\left(\mu_d\right)=\int_0^1 f_D\left(\mu_d,\eta_D\right)d\eta_D. \tag{A30}$$

It is assumed that the energy dissipation of SDCs is independent of the pinching behavior of the surrounding RC beams, as shown in the right panel of Supplemental Figure 2. Therefore, $f_D\left(\mu_d,\eta_D\right)$ is calculated such that

$$f_D(\mu_d,\eta_D)=\begin{cases}\frac{1}{2}{\mu_d}^2\left(1-{\eta_D}^2\right) & 0\le\mu_d\le 1\\ \mu_d-\frac{1}{2}\left\{1+(\eta_D\mu_d)^2\right\} & \mu_d\ge 1 \text{ and } 0\le\eta_D\le\frac{1}{\mu_d}\\ (1+\eta_D)\mu_d-2 & \mu_d\ge 1 \text{ and } \frac{1}{\mu_d}\le\eta_D\le 1\end{cases}. \tag{A31}$$

By substituting Eq. (A31) into Eq. (A30), the function $\widetilde{f_D}(\mu_d)$ is calculated as shown in Eq. (A32):

$$\widetilde{f_D}(\mu_d)=\begin{cases}\frac{1}{3}{\mu_d}^2 & 0\le\mu_d\le 1\\ \frac{1}{6}\left(9\mu_d-12+\frac{5}{\mu_d}\right) & \mu_d\ge 1\end{cases}. \tag{A32}$$

The contribution of the viscous damping is calculated using Eq. (A33), as in Fujii and Shioda (2023):

$$\frac{\Delta E_{D1}^*}{M_1^*}=\frac{7\pi h_{1f\max}}{12}A_{1f\ \max}^*D_{1\ \max}^*, \tag{A33}$$

where $h_{1f\max}$ is the damping ratio corresponding to the peak equivalent displacement ($D_{1\ \max}^*$) and $A_{1f\ \max}^*$ is the contribution of the RC MRF to the equivalent acceleration at $D_{1\ \max}^*$. In Fujii and Shioda (2023), $h_{1f\max}$ is assumed to be proportional to the secant circular frequency of the first mode of the RC MRF, corresponding to $D_{1\ \max}^*$. Therefore, $h_{1f\max}$ is calculated as:

$$h_{1f\max}=\frac{\omega_{1f\max}}{{}_1\omega_{1f}}h_{1f}=\frac{1}{{}_1\omega_{1f}}\sqrt{\frac{A_{1f\ \max}^*}{D_{1\ \max}^*}}h_{1f}, \tag{A34}$$

In Eq. (A34), ${}_1\omega_{1f}$ and $\omega_{1f\max}$ are the secant circular frequency of the first mode of RC MRF corresponding to the initial stage and $D_{1\ \max}^*$, respectively.